Atmos. Chem. Phys. Discuss., 9, 9457–9489, 2009
www.atmos-chem-phys-discuss.net/9/9457/2009/

Atmospheric Chemistry and Physics Discussions

This discussion paper is/has been under review for the journal *Atmospheric Chemistry and Physics (ACP)*. Please refer to the corresponding final paper in *ACP* if available.

Modeling of secondary organic aerosol yields from laboratory chamber data

M. N. Chan[1], A. W. H. Chan[2], P. S. Chhabra[2], J. D. Surratt[2], and J. H. Seinfeld[1,2]

[1]Division of Engineering and Applied Science, California Institute of Technology, Pasadena, CA, USA
[2]Division of Chemistry and Chemical Engineering, California Institute of Technology, Pasadena, CA, USA

Received: 19 March 2009 – Accepted: 24 March 2009 – Published: 9 April 2009

Correspondence to: J. H. Seinfeld (seinfeld@caltech.edu)

Published by Copernicus Publications on behalf of the European Geosciences Union.

Abstract

A product-specific model for secondary organic aerosol (SOA) formation and composition based on equilibrium gas-particle partitioning is evaluated. The model is applied to represent laboratory data on the ozonolysis of α-pinene under dry, dark, and low-NO_x conditions in the presence of ammonium sulfate seed aerosol. Using five major identified products, the model is fit to the chamber data. From the optimal fitting, SOA oxygen-to-carbon (O/C) and hydrogen-to-carbon (H/C) ratios are modeled. The discrepancy between measured H/C ratios and those based on the oxidation products used in the model fitting suggests the potential importance of particle-phase reactions. Data fitting is also carried out using the volatility basis set, wherein oxidation products are parsed into volatility bins. The product-specific model is best used for an SOA precursor for which a substantial fraction of the aerosol-phase oxidation products has been identified.

1 Introduction

Laboratory chamber data are needed to determine secondary organic aerosol (SOA) yields from volatile organic compounds (VOCs). The fundamental concept on which all descriptions of SOA formation lies is that SOA comprises a mixture of semivolatile organic compounds that partition between the gas and particle phases (Pankow, 1994a,b; Odum et al., 1996). Gas-particle partitioning of each compound is described by an equilibrium partitioning coefficient, K_p,

$$K_p = \frac{P}{GM} \sim \frac{1}{c^*}, \quad (1)$$

where G is the mass concentration per unit volume of air ($\mu g\,m^{-3}$) of the semivolatile species in the gas phase, P is the mass concentration per unit volume of air ($\mu g\,m^{-3}$) of the semivolatile species in the particle phase, and M is the mass concentration per unit

ACPD
9, 9457–9489, 2009

volume of air ($\mu g\,m^{-3}$) of the total absorbing particle phase. The equilibrium partitioning coefficient, K_p ($m^3\,\mu g^{-1}$), is inversely proportional to the saturation vapor concentration, c^* ($\mu g\,m^{-3}$), of the pure semivolatile compound (see Appendix A). M refers only to the portion of the particulate matter participating in absorptive partitioning (organic aerosol into which semivolatile organics can partition and the aqueous portion of the particles in the case of water-soluble organics). Note that as long as some absorbing mass is present, some fraction of a given semivolatile compound partitions into the particle phase, even if its gas-phase concentration is below its saturation vapor concentration, c^*.

Oxidation of a parent VOC leads to a variety of semivolatile products, each with its own saturation vapor concentration. Moreover, the semivolatile oxidation products may be formed from first- or higher generation gas-phase reactions, and the products themselves may react further in the gas phase to yield compounds of either lower (in the case of addition of more functional groups) or greater (in the case in which the carbon backbone of the molecule is cleaved) volatility.

The fraction F of a semivolatile compound in the particle phase can be expressed in term of K_p or c^* as

$$F = \frac{P}{G+P} = \frac{MK_p}{1+MK_p} = \frac{1}{1+c^*/M} \,. \tag{2}$$

As the amount of absorbing material (M) increases, compounds of greater volatility (larger c^*, smaller K_p) will partition increasingly into the particle phase. When $c^*=M$, half of the semivolatile mass resides in the particle phase. If $M \gg c^*$, essentially all of the semivolatile species is in the particle phase.

In the first basic model of SOA formation, Odum et al. (1996) represented the process of SOA formation by n semivolatile products and showed that the SOA yield Y, defined as the mass of aerosol formed per mass of hydrocarbon reacted, can be ex-

pressed as

$$Y = M \sum_i \frac{\alpha_i K_{p,i}}{1 + M K_{p,i}}, \quad (3)$$

where α_i is the mass-based stoichiometric coefficient for product i (mass of i produced per mass of parent VOC reacted). Note that Y can exceed 1.0 as a result of the increase of molecular mass of oxidation products. (The designation "aerosol mass fraction" is also used for Y.) Equation (3) is an equilibrium model in that it relates the amount of each product formed to the amount of VOC reacted regardless of whether the processes occurs in a single or multiple chemical steps in the gas phase. While, in principle, n can be as large as desired, in the application of the Odum model is usually n=2. The two products are not necessarily associated with actual products, and the 4 parameters, $\alpha_1, \alpha_2, K_{p,1}$, and $K_{p,2}$, are estimated by optimal fitting of Eq. (3) to the data.

SOA forms when gas-phase oxidation products of a hydrocarbon precursor partition between the gas and particle phases. Products with lower vapor pressures partition preferentially to the particle phase; compounds that are more highly oxygenated tend to have lower vapor pressures. The degree of partitioning to the particle phase depends also on the quantity of absorbing organic material in that phase into which the compounds can condense; as the mass of absorbing material increases, compounds of higher vapor pressure that tend not to partition to the particle phase under low mass loadings do so at the higher mass loadings. The result is that SOA at low mass loading tends to be enriched in the least volatile (and most oxygenated) products (Bahreini et al., 2005; Shilling et al., 2008). In typical chamber experiments, a range of initial hydrocarbon precursor concentrations is employed in order to determine SOA yields as a function of the mass concentration of organic particles generated. When chamber experiments are conducted over a range of initial VOC concentrations, such experiments afford a view of the full spectrum of oxidation products, thereby facilitating the formulation of chemical mechanisms.

Laboratory chamber studies are limited in duration to about 12 h or so, as constrained by particle deposition on the chamber walls, whereas the typical atmospheric lifetime of a particle is the order of a week. Chamber studies capture the initial multi-hour VOC oxidation but not that which takes place on a multi-day time scale. The sequence of reactions and associated SOA formation that occur over the duration of a chamber experiment can be termed as the *chamber phase*. (Stanier et al., 2008, have referred to this as the "prompt" phase.) The chamber or prompt phase chemistry begins with oxidant (OH, O_3, NO_3) attack on the VOC, initiating a series of reactions, which can depend critically on NO_x level, leading to semivolatile products. Experimentally-derived SOA yields reflect the extent of SOA formation over the chamber phase. Reactions that occur on a time scale longer than a chamber experiment can be termed the *aging phase*, during which the following processes may occur: (1) particle-phase accretion reactions that convert semivolatile condensed products to essentially non-volatile compounds; (2) gas-phase oxidation reactions of chamber phase semivolatile products that are too slow to be important during the chamber phase but are capable of producing compounds of even lower volatility over the aging phase; and (3) gas-particle reactions that convert some particulate material to volatile products. Over the typical time scale and spatial grid scale of atmospheric models, SOA formation occurring on the chamber phase time scale can be considered as taking place essentially instantaneously, suggesting that an equilibrium partitioning model for this phase is appropriate. Over the longer aging time scale, the equilibrium partitioning can be considered to be slowly perturbed as chemical aging takes place.

2 Form of SOA model

If a number of products accounting for a significant fraction of the total mass of SOA have been identified, these major products can serve as SOA surrogates in a product-specific model. In the product-specific model (Pankow et al., 2001; Seinfeld et al., 2001), if the vapor pressures can be estimated, the values of K_p of the major products

can be determined. One must keep in mind the fact that vapor pressure estimation methods for highly oxygenated SOA compounds may involve considerable uncertainty.

An alternative approach is the *volatility basis set*, in which a range of products is specified in terms of volatility bins (Donahue et al., 2006; Stanier et al., 2008). The product volatilities can be segmented into order-of-magnitude volatility bins (expressed as values of c^*). Since SOA products are grouped into volatility bins, information about the chemical composition of SOA is not required.

For the volatility basis set, Stanier et al. (2008) present a methodology for selecting the maximum and minimum values of c^*, and logarithmic spacing between c^* values then determines the number of volatility bins. For the product-specific model, major identified particle-phase products are chosen as SOA surrogates to represent other chemically similar compounds, and to give a reasonable approximation of gas/particle partitioning of all other products (Pankow et al., 2001). The product-specific model allows the composition of SOA to be predicted. The simulated SOA composition may allow a first approximation of the properties of SOA (e.g., water uptake and cloud condensation nuclei activity).

Here, we revise the product-specific model proposed by Pankow et al. (2001) in which the SOA yield and composition can be modeled by using absorptive gas/particle partitioning of major SOA products. The SOA composition changes with organic mass loading and the amount of hydrocarbon precursors reacted can be tracked. Using the simulated SOA composition, we also calculate the aerosol oxygen-to-carbon (O/C) and hydrogen-to-carbon (H/C) ratios at different loadings. Simulated ratios for O/C and H/C can be compared with those measured. As an illustration of this approach, we examine the ozonolysis of α-pinene under dry, dark, and low-NO_x conditions in the presence of dry $(NH_4)_2SO_4$ particles.

3 Ozonolysis of α-pinene

Ozonolysis of α-pinene is, in many respects, an excellent test case for an SOA model. A number of experimental studies exist in the literature, and relatively complete product identification has been carried out. Oxocarboxylic acids, hydroxy oxocarboxylic acids, dicarboxylic acids, oxoaldehydes, and organic peroxides are the major classes of SOA products identified (Yu et al., 1999; Docherty et al., 2005). We assume for the product-specific model that there are five major products: pinonic acid, pinic acid, pinonaldehyde, a hydroperoxide, and terpenylic acid (Table 1). These compounds are chosen to reflect the latest understanding of the gas-phase products formed in the ozonolysis of α-pinene.

Gas-particle partitioning of compounds are determined by their vapor pressures. Here, the vapor pressure of a product i is estimated by using a group contribution method developed by Pankow and Asher (2008). At a given temperature, the $K_{p,i}$ of the product i is determined by assuming that its activity coefficient, ζ_i, is unity and the molecular weight of product i is taken as the mean molecular weight of the surrogate mixture, $\overline{\mathrm{MW}}$, as a first approximation. These assumptions may be reasonable as the range of molecular weights of products is small (168–200 g mol^{-1}, see Table 1) and the amount of water present in the particle phase is not significant under dry conditions (<5%–40% RH). Bilde and Pandis (2001) measured the vapor pressure of semivolatile products formed from oxidation of biogenic monoterpenes using a laminar flow reactor with uncertainty of ±50%. They reported a vapor pressure of 1.989×10^{-10} atm for pinic acid of at 293 K, which is comparable to our estimated value (4.605×10^{-10} atm) using the Pankow and Asher (2008) model. At a given temperature, our estimated vapor pressures of major products are lower than those estimated by Jenkin (2004). Hence, our estimated K_p values of major products are larger than those reported by Jenkin (2004). It is noted that Jenkin (2004) estimated a higher vapor pressure of pinic acid of 4.7×10^{-4} torr (or 6.18×10^{-7} atm) at 298 K compared to that reported by Bilde and Pandis (2001) (4.213×10^{-10} atm).

Some of the products are estimated to have very similar K_p values at a given temperature. For example, at 293 K, the estimated value of K_p of hydroxy pinonic acid (K_p=0.2802) is very close to that of pinic acid (K_p=0.2822). The estimated K_p of pinonic acid (K_p=0.0017) is close to that of hydroxy pinonaldehyde (K_p=0.0018). As a result, any optimization will not be able to differentiate between these products. In these cases, a single product is chosen to represent the two classes of products. By considering the similarity of the K_p values and the relative abundance of these species, pinonic acid is chosen to represent the pinonic acid, norpinonic acid, hydroxy pinonaldehyde, and isomers. Pinic acid is chosen to represent pinic acid, norpinonic acid, hydroxy pinonic acid, and isomers.

In practical terms, the constraints imposed by chamber data are reflected in the optimal fitting of parameters in any model to chamber data. The basic chamber data are considered to be in the form of particle mass concentration as a function of VOC reacted. The actual chamber data are in the form of aerosol volume concentration. Aerosol density needed to convert volume to mass concentration is estimated by comparing the aerosol number distribution measured by a differential mobility analyzer with that obtained from the Aerodyne Aerosol Mass Spectrometer (AMS), through the theoretical relationship between mobility diameter and vacuum aerodynamic diameter. Ng et al. (2006) have shown that for the oxidation of a number of hydrocarbons with a single double bond, the growth curve for one experiment over the course of the experiment ("time dependent growth curve") follows that of final SOA growth over different experiments. This suggests that in this case the time-dependent SOA growth data can also be used for model data fitting.

Data from ozonolysis of α-pinene are obtained from experiments conducted under dry, dark, and low-NO_x conditions in the presence of dry $(NH_4)_2SO_4$ particles (Ng et al., 2006; Pathak et al., 2007; Shilling et al., 2008). The SOA yield data cover a range of organic mass loading (0.5–411 $\mu g\,m^{-3}$) and are used for the parameterization to model the SOA yield relevant to atmospheric conditions (Presto and Donahue, 2006). An effective SOA density of 1.25 $g\,cm^{-3}$ is applied for conversion of volume to mass con-

centration in determination of SOA yield. It is noted that Shilling et al. (2009) reported a higher effective SOA density (1.73–1.4 g cm^{-3}) at low organic mass loading (0.5–7 µg m^{-3}). The SOA yield data from Shilling et al. (2008) are adjusted to 293 K, using a temperature correction factor suggested by Pathak et al. (2007). Generally, the time-dependent SOA yield data reported by Ng et al. (2006) are in good agreement with the final SOA yield data reported by Pathak et al. (2007) and Shilling et al. (2008) but are lower than those reported by Shilling et al. (2008) for organic mass loadings less than 2 µg m^{-3}. Measurement uncertainties may explain part of the variability in SOA yield data reported by Ng et al. (2006) at low organic mass loading.

Data, plotted as SOA yield, Y versus organic mass loading, M, are shown in Fig. 1. The SOA yield increases rapidly at low organic mass loading and more slowly at high organic mass loading. Since any vapor pressure estimation method for SOA compounds may have considerable uncertainty, the estimated value of $K_{p,i}$ of a product i may have a correspondingly large uncertainty. The value of $K_{p,i}$ of all products is multiplied by a factor of 100 to examine the effect of uncertainty in determination of $K_{p,i}$ (termed the $K_p \times 100$ case). Previous modeling studies have shown that an overall increase of K_p of all products of a factor on the order of 10^2 is needed to explain the partitioning (Jenkin, 2004; Chen and Griffin, 2005). The α_i of the product i is then obtained by optimal fitting to the experimental SOA yield data in both $K_p \times 1$ and $K_p \times 100$ cases. The predicted SOA yields agree well with the experimental SOA yield data in both $K_p \times 1$ and $K_p \times 100$ cases. The $K_p \times 100$ case gives a better estimate of SOA yields at low organic mass loading than the $K_p \times 1$ case. However, the optimized curves underpredict the SOA yield data reported by Shilling et al. (2008) when organic mass loading is less than ~2 µg m^{-3}. One possible explanation is the uncertainty in the estimation of the K_p of major products (vapor pressure and activity coefficient). Another possible explanation is that products (gas-phase and/or particle-phase) of higher K_p (and lower volatilities) not considered in the model are present. Once gas-phase reaction products partition into the particle-phase, they may undergo further reaction. Particle-phase reaction products (e.g., oligomers and esters) tend to have higher molecular weights and

lower volatilities (Gao et al., 2004; Iinuma et al., 2004; Müller et al., 2008), therefore enhancing the K_p of gas-phase reaction products (Kroll and Seinfeld, 2005). Table 1 lists the parameters used to describe the experimental SOA yields. It is acknowledged that the mass yield of pinonaldehyde is close to unity in both $K_p \times 1$ and $K_p \times 100$ cases. For the $K_p \times 1$ case, the sum of fitted molar yields exceeds 1.

The volatility basis set is also applied to fit the experimental SOA yields. The estimated volatility (or c^*) of products spans from 0.035 to 873 $\mu g\,m^{-3}$. A volatility basis set of six volatility bins is chosen and the volatility bins are separated by an order-of-magnitude (c^*: 0.01, 0.1, 1, 10, 100, and 1000 $\mu g\,m^{-3}$). The mass of aerosol in bin i is obtained by optimal fitting to the experimental SOA yield data. Figure 1 shows that for the volatility basis set, the predicted SOA yields agree well with the experimental SOA yield data, even at low organic mass loading ($<0.5\,\mu g\,m^{-3}$). This suggests that products with volatility as low as $c^*=0.01\,\mu g\,m^{-3}$ (or $K_p=100\,\mu g^{-1}\,m^3$) are present. The quantity of aerosol in the volatility bin i is in good agreement with that of the product i with similar K_p or c^* (Table 1) in the $K_p \times 100$ case.

We also investigate temperature dependence of SOA yield using the product-specific model (only the $K_p \times 100$ case which gives a better description of SOA yields is shown). The temperature-dependent vapor pressure of the products can be estimated using the group contribution method developed by Pankow and Asher (2008). At a given temperature, $K_{p,i}$ of the product i is also estimated by assuming that its ζ_i is unity and the molecular weight of product i is taken as the mean molecular weight of the absorbing phase. The α_i of the product i determined at 293 K is assumed to be temperature independent over the temperature range studied (273–313 K). As shown in Fig. 2, the predicted SOA yield increases as the temperature decreases. Lower temperature tends to favor the partitioning of gas-phase reaction products into the particle phase, resulting in a higher SOA yield. Pathak et al. (2007) observed a weak dependence of SOA yield on temperature. The SOA yields change slightly when the temperature increases from 288 to 313 K. The model predicts a stronger temperature dependence of SOA yield than observed. The predicted SOA yields agree well with those measured

at 293 and 303 K. On the other hand, the predicted SOA yields are higher than those measured at 288 and 273 K but slightly lower than those measured at 313 K.

4 SOA composition

At a given temperature and organic mass loading, M the mass yield of the product i, Y_i can be determined as:

$$Y_i = \frac{M_i}{\Delta HC} = \frac{MK_{p,i}}{1 + MK_{p,i}}\alpha_i \,, \tag{4}$$

where the mass-based stoichiometric coefficient of the product i, Y_i, is obtained from the parameterization of SOA yield data using the product-specific model (Table 1). M_i is the concentration of product i in the particle phase ($\mu g\,m^{-3}$). The SOA yield, Y, is the sum of the mass yields of all products (SOA yield, $Y = \sum_i Y_i$, at a given organic mass loading. The ratio of mass yield of product i to total yield (Y_i/Y) is the relative contribution of the product i to the total SOA yield (or total SOA mass).)

Figures 3 and 4 show the predicted relative contributions of the products to the SOA yield at different organic mass loading for the $K_p \times 1$ and $K_p \times 100$ cases, respectively. The predicted SOA composition is compared to the measured concentration of the corresponding classes of compounds in chamber experiments. Yu et al. (1999) reported the product distribution of ozonolysis of α-pinene at 306 K and organic mass loading of 38.8 $\mu g\,m^{-3}$: hydroxy pinonic acid (17.7%), pinic acid and norpinic acid (22.5%), pinonic acid and norpinonic acid, and isomers (36.5%), hydroxy pinonaldehyde (15.9%), and pinonaldehyde and norpinonaldehyde (7.4%). It is noted that organic peroxides, particle-phase reaction products (e.g., oligomers and esters), and terpenylic acid were not reported in Yu et al. (1999). Docherty et al. (2005) estimated that organic peroxides contribute ~47% of the SOA mass at high organic mass loading. The concentration of terpenylic acid in chamber SOA has not been reported previously by Claeys et al. (2009). A smaller effective density of 1 $g\,cm^{-3}$ used to calculate

the SOA mass in Yu et al. (1999). This will increase the reported percentage of products. In addition, the relative abundance of products reported by Yu et al. (1999) may be overestimated if the organic peroxides, terpenylic acid, or other unidentified products contribute significantly to the SOA mass at the given organic mass loading.

As shown in the bottom panel of Fig. 3, for the $K_p \times 1$ case, only pinic acid and pinonic acid are predicted to contribute significantly to the SOA mass. Other major products are estimated to be too volatile to partition into the particle phase and thus contribute only a very small fraction of SOA mass. This also explains why high mass yields of these products are needed in order to fit the observed SOA yields. Generally, the simulated SOA composition does not match those measured. As shown in the bottom panel of Fig. 4, for the $K_p \times 100$ case, the predicted percentage of pinonic acid is about 51%, which is close to the sum of the percentages of pinonic acid and norpinonic acid and isomers and hydroxy pinonaldehyde (52.4%). The predicted percentage of pinonaldehyde is also close to that of pinonaldehyde and norpinonaldehyde (7.4%). On the other hand, the predicted percentage of pinic acid is about 28%, which is smaller than the sum of the percentages of pinic acid and norpinic acid and hydroxy pinonic acid (40.2%). For organic peroxides, using a hydroperoxide as surrogate gives ~7% of SOA yield, which is lower than that reported by Docherty et al. (2005) at high organic mass loading. The percentage of terpenylic acid contributes about 5% of the SOA yield. Overall, the $K_p \times 100$ case may give a good first estimate of the gas/particle partitioning and composition of the SOA products at the given organic mass loading and temperature.

5 O/C and H/C ratios

The chemical composition of SOA formed from ozonolysis of α-pinene has been recently characterized by an Aerodyne high-resolution time-of-flight aerosol mass spectrometer (HR-ToF-AMS) at 298 K (Shilling et al., 2009). This characterization provides measurement of the O/C and H/C ratios at different organic mass loadings; these data

provide additional information about the SOA composition and impose important constraints on the SOA parameterization. As shown in Figs. 5 and 6, the data show that the O/C ratio decreases as the organic mass loading increases, while the H/C ratio increases (Shilling et al., 2009). This observation indicates, as expected, that the SOA is more oxygenated at low organic mass loading than at high organic mass loading.

O/C and H/C ratios of the SOA can also be determined from the predicted SOA composition. At a given organic mass loading, the number of moles of product i, m_i can be calculated from its particle-phase mass concentration and molecular weight. The number of carbon atoms, $n_{C,i}$, $(O/C)_i$ and $(H/C)_i$ ratios of the product i are known (Table 1). The O/C and H/C ratios of the SOA can be determined as follows:

$$O/C = \frac{\sum_i m_i \cdot n_{c,i} \cdot (O/C)_i}{\sum_i m_i \cdot n_{c,i}}, \quad (5)$$

$$H/C = \frac{\sum_i m_i \cdot n_{c,i} \cdot (H/C)_i}{\sum_i m_i \cdot n_{c,i}}. \quad (6)$$

At 298 K, for the $K_p \times 1$ case (Fig. 5, top panel), the modeled O/C ratios decrease from ~0.44 to ~0.36 as the organic mass loading increases from 0.5 $\mu g\,m^{-3}$ to 150 $\mu g\,m^{-3}$. The predicted O/C ratios are higher than those in Shilling et al. (2009), except at low organic mass loading (<1 $\mu g\,m^{-3}$). The predicted ratios decrease less rapidly as the organic mass loading increases. For the $K_p \times 100$ case (Fig. 5, bottom panel), the predicted O/C ratios agree quite well with those measured; predicted O/C ratios decrease from 0.43 to 0.30 as the organic mass loading increases. On the other hand, in both $K_p \times 1$ and $K_p \times 100$ cases, the predicted H/C ratios exceed those measured at these loadings (Fig. 6).

The O/C ratios of selected major products range from 0.2 to 0.5, which cover the range of the experimental O/C ratios. On the other hand, the H/C ratios of the selected major products range from 1.5 to 1.6, which exceed the reported H/C ratios (1.38–1.51). Using the experimentally identified gas-phase reaction products, the predicted H/C ratios do not match those reported at low organic mass loading. Notably, the H/C

ratios of the major SOA products identified in the literature range from 1.5 to 1.6. In addition to uncertainties in determination of the O/C and H/C ratios, the formation of oligomers or organic peroxides will shift the H/C ratio without greatly affecting the O/C ratio (Shilling et al., 2009). Formation of esters can alter the H/C and O/C ratios (Müller et al., 2008). The discrepancy in the H/C ratios based on known gas-phase products and those measured stresses the potential importance of particle-phase reactions on the determination of SOA yield and composition in the ozonolysis of α-pinene under dry, dark, and low-NO_x conditions.

Figures 5 and 6 also show the temperature dependence of the H/C and O/C ratios in the temperature range (273–313 K). For the both $K_p \times 1$ and $K_p \times 100$ cases (Fig. 5), the modeled O/C ratio increases when the temperature increases. On the other hand, the modeled H/C ratio decreases when the temperature increases (Fig. 6). At a higher temperature, the less volatile gas-phase products which are usually more oxygenated (i.e., usually a higher O/C ratio and a lower H/C ratio) partition preferentially into the particle phase. As shown in Fig. 4 ($K_p \times 100$ case), the contribution of pinic acid, which is the least volatile product and is more oxygenated, increases when the temperature increases from 293 to 306 K. On the other hand, the relative abundance of pinonaldehyde, which is the most volatile product and is the least oxygenated, decreases with increasing temperature. The effect of particle-phase reactions on O/C and H/C ratios at different temperatures is not considered. For the volatility basis set, since information about the chemical composition of volatility bins is not required, O/C and H/C ratios cannot be directly determined from the quantity of aerosol in the bins. With a priori knowledge of the SOA composition, the O/C and H/C ratios of the bins can be obtained from the optimal fitting to the measured O/C and H/C ratios (Shilling et al., 2009).

We conducted an α-pinene ozonolysis experiment under dry, dark, and low-NO_x conditions in the presence of dry $(NH_4)_2SO_4$ particles to generate a data set comparable to that of Shilling et al. (2008, 2009). The chemical composition of the SOA was continuously monitored using an Aerodyne HR-ToF-AMS. Details of the experiment

are given in Appendix B. Figure 7 shows the time evolution of α-pinene concentration, organic mass loading, and aerosol O/C and H/C ratios. Once the ozone is injected, α-pinene oxidation commences, and the organic mass loading increases almost immediately. When α-pinene is completely reacted, organic aerosol mass loading remains unchanged. These observations are consistent with those reported by Ng et al. (2006).

Measured O/C and H/C ratios as a function of organic mass loading are shown in Fig. 8. The data scatter reflects the inherent uncertainty in measurement of O/C and H/C ratios at low organic mass loading. Generally, the H/C ratio increases as time increases, while the O/C ratio decreases. The trends in O/C and H/C ratios are in good agreement with those reported by Shilling et al. (2009). The absolute values of the O/C ratios are slightly lower than those reported by Shilling et al. (2009), but well within the experimental uncertainty. When all α-pinene is consumed and the SOA growth has leveled out ($\sim$58 $\mu g\,m^{-3}$), O/C and H/C ratios and fragment mass spectrum (not shown here) remain unchanged. As discussed by Ng et al. (2006), the first oxidation step in the ozonolysis of α-pinene (a hydrocarbon with a single double bond) is most likely the rate-determining step in SOA formation. Either the condensable products are the initial reaction products of the parent hydrocarbon oxidation (first-or higher generation products), or subsequent reactions (in either the gas or particle phase) proceed at relatively fast rates. Thus, the instantaneous product spectrum can be considered as that at equilibrium during the chamber phase.

Recently, Dzepina et al. (2009) suggest that the O/C ratio and volatility can be used to compare modeled and measured SOA. The authors calculate O/C ratios using various models and compare these to the measured O/C ratios of ambient Mexico City aerosol. They find that O/C ratios predicted by different models do not agree and are generally lower than the measured ratios.

In the present study, we show that although good agreement in O/C ratio between observations and predictions can exist, a discrepancy in H/C ratio can exist. Hence, in addition to the O/C ratio, other element-to-carbon ratios such as H/C are important for modeling fitting and comparison. S/C and N/C ratios could be used once accurate

determinations can be made using the AMS. These element-to-carbon ratios can also be calculated using detailed gas-chemistry models coupled with gas/particle partitioning theory and can be used as additional constraints on the SOA parameterization in chamber experiments and modeling studies.

6 Discussion

Clear evidence exists that organic compounds may undergo chemical reactions in the particle phase, changing the concentration and/or volatility of the compounds (Kroll and Seinfeld, 2008, and references therein). Particle-phase reaction products can contribute a significant fraction of the total SOA mass, suggesting that processes governing the amount of SOA formed may be more complex than the direct formation and condensation of semivolatile organic compounds. Kroll and Seinfeld (2005) have introduced effective partitioning coefficients, which account for both absorption and particle-phase reaction to represent the enhancement in the partitioning of semivolatile products into the particle-phase. Heterogeneous and particle-phase reactions have been considered in some SOA models (Hallquist et al., 2009, and references therein). Major challenges exist in the development of explicit SOA models coupling both detailed gas-phase and particle-phase reactions.

The equilibrium partitioning model can be used to describe the gas-particle partitioning of the SOA products, including particle-phase reaction products. The traditional absorptive partitioning model treats the α_i as the total product yield of each product formed from single or multiple generations of reaction in the gas-phase. In the presence of particle-phase reactions, the definition of α can be expanded to refer to the overall product yield from the entire reaction mechanism. In this case, major particle-phase reaction products can also be chosen as SOA surrogates in the product-specific model. The vapor pressures and gas-particle partition coefficients of particle-phase reaction products can likewise be estimated. The α_i values for the SOA surrogates (gas-phase or/and particle phase) can then be obtained from fitting of chamber data.

This simple treatment has the potential to reproduce the measured concentrations of major reaction products (both gas-phase and particle-phase) even in the absence of details of major particle-phase reactions. On the other hand, if an equilibrium state is not attained during the chamber phase, the kinetics of gas-phase and particle-phase reactions determine the SOA composition. In such cases, development of kinetic models in which reaction products undergo reactions in both gas-phase and particle-phase is needed to describe the SOA formation (Chan et al., 2007).

To determine the extent to which an equilibrium state is achieved, the chemical composition of SOA can be measured by the Aerodyne HR-ToF-AMS over the course of the chamber experiments. The change in element-to-carbon ratios (e.g. O/C, H/C ratios) can provide insight about the change in SOA composition. If the ratios or the mass spectra do not vary with time, this may suggest that an equilibrium state is achieved within the timescale of the chamber experiment. In that case, major experimentally identified products (both particle-phase and gas-phase reaction products) can be chosen as SOA surrogates in the product-specific model. In addition, the O/C, H/C, N/C, or S/C ratios can be calculated from the detailed gas-chemistry model coupled with gas/particle partitioning theory.

Appendix A

The gas-particle partitioning coefficient

The gas-particle partitioning coefficient for compound i to a condensed phase of i only is given by (Pankow, 1994a,b)

$$K_{p,i} = \frac{RT}{10^6 \mathrm{MW}_i p^o_{L,i}}, \quad \text{(A1)}$$

where R=8.2×10^{-5} m^3 atm mol^{-1} K^{-1}, MW$_i$=molecular weight of i (g mol^{-1}) and $p^o_{L,i}$ is the vapor pressure of pure i as a liquid (atm). When multiple condensed-phase

compounds exists

$$K_{p,i} = \frac{RTf}{10^6 \overline{\mathrm{MW}} \zeta_i p^o_{L,i}} , \quad \text{(A2)}$$

where f=weight fraction of the total particulate matter that is the absorbing phase, $\overline{\mathrm{MW}}$ is the mean molecular weight of the absorbing organic phase (g mol^{-1}), and ζ_i=mole-fraction based activity coefficient. $K_{p,i}$ varies as a function of T, through both its explicit dependence on T as well as the strong dependence $p^o_{L,i}$ of on T. The value of $K_{p,i}$ is also influenced by ζ_i and $\overline{\mathrm{MW}}$ owing to the types and amounts of condensed-phase compounds.

The vapor pressure of each component obeys the Clausius-Clapeyron equation,

$$p^o_{L,i}(T) = p^o_{L,i} \exp\left[-\frac{\Delta H_{v,i}}{R}\left(\frac{1}{T} - \frac{1}{T_o}\right)\right] . \quad \text{(A3)}$$

For a set of compounds at a given T, $p^o_{L,i}$ tends to decrease with increasing $\Delta H_{v,i}$.

The variation of gas-partitioning coefficient with temperature results from variation of $p^o_{L,i}$ as well as the explicit dependence on T,

$$\frac{K_{p,i}(T)}{K_{p,i}(T_o)} = \left(\frac{T}{T_o}\right)\frac{p^o_{L,i}(T_o)}{p^o_{L,i}(T)} = \left(\frac{T}{T_o}\right)\exp\left[-\frac{\Delta H_{v,i}}{R}\left(\frac{1}{T} - \frac{1}{T_o}\right)\right] . \quad \text{(A4)}$$

Following Pankow and Chang (2008), one may choose ΔH_v=100 kJ mol^{-1} as a "reference" $\Delta H_{v,i}$ value of, so that any $\Delta H_{v,i}$ can be written as a multiple of the reference value, $\Delta H_{v,i}$=a_i×100 kJ mol^{-1}. For T_o=293 K, for, a=1, a 10 K decrease in T leads to

$$\frac{K_{p,i}(283)}{K_{p,i}(293)} = \left(\frac{283}{293}\right)\exp\left[-\frac{100}{R}\left(\frac{1}{283} - \frac{1}{293}\right)\right] = 4.1 . \quad \text{(A5)}$$

Thus, for a compound with ΔH_v=100 kJ mol^{-1}, a 10 K decrease in temperature leads to a factor of 4 increase in $K_{p,i}$. For a compound with a_i=0.5, the increase of $K_{p,i}$ for a 10 K decrease in T is ~ a factor of 2. Note that the factor (T/T_o) exerts only a minor effect compared to that from the temperature dependence of $p^o_{L,i}$.

Appendix B

Measurement of O/C and H/C ratios of SOA from α-pinene ozonolysis

To provide an additional set of data on the O/C ratio of SOA generated from α-pinene ozonolysis, an experiment was performed in one of the dual Caltech 28-m^3 Teflon chambers. Details of the facility have been described elsewhere (Cocker et al., 2001; Keywood et al., 2004). Before the experiment, the chamber was flushed continuously with dry, purified air for at least 24 h. Aerosol number concentration, size distribution, and volume concentrations were measured by a differential mobility analyzer (DMA, TSI model 3081) coupled with a condensation nucleus counter (TSI model 3760). Ammonium sulfate seed particles were generated by atomizing an aqueous solution of 0.015 M $(NH_4)_2SO_4$ with a constant-rate atomizer. The volume concentration of the seed particles was 12 µm^3 cm^{-3}.

The parent hydrocarbon, α-pinene, and an OH scavenger, cyclohexane, were then introduced separately by injecting known volumes of the liquid hydrocarbon into a glass bulb, subsequently carried into the chamber by an air stream at 5 L min^{-1}. The mixing ratio of α-pinene was monitored with a gas chromatograph coupled with a flame ionization detector (GC-FID, Agilent model 6890N). The initial mixing ratio of α-pinene was 44 ppb. The estimated mixing ratio of cyclohexane was 37 ppm, which corresponds to a rate of cyclohexane + OH 100 times faster than that of α-pinene + OH.

Ozone was generated with a UV lamp ozone generator (EnMet Corporation, MI),

and monitored with a commercial ozone analyzer (Horiba Instruments, CA). Ozone injection was stopped after the ozone concentration reached 180 ppb. The aerosol growth data were corrected for wall deposition of particles. First-order size dependent wall loss coefficents were determined from a separate seed-only experiment. The final SOA volume was 46 $\mu m^3\,cm^{-3}$, as measured by the DMA.

Real-time particle mass spectra were collected continuously by an Aerodyne High Resolution Time-of-Flight Aerosol Mass Spectrometer (HR-ToF-AMS). The HR-ToF-AMS is described in detail elsewhere (Canagaratna et al., 2007, and references therein). The HR-ToF-AMS switched once every minute between the high resolution W-mode and the lower resolution, higher sensitivity V-mode. The V-mode data were analyzed using a fragmentation table to separate sulfate, ammonium, and organic spectra and to time-trace specific mass-to-charge ratios. W-mode data were analyzed using a separate high-resolution spectra toolbox known as PIKA to determine the chemical formulas contributing to distinct mass-to-charge ratios (DeCarlo et al., 2006).

To determine elemental ratios, the computational toolbox Analytical Procedure for Elemental Separation (APES) was used. This toolbox applies the analysis procedure described in Aiken et al. (2007) to the high-resolution W-mode data. The particle-phase signal of CO^+ and the organic contribution to H_xO^+ ions were estimated as described in Aiken et al. (2008).

Acknowledgements. This work was supported by the Office of Science (BER), US Department of Energy, Grant No. DE-FG02-05ER63983 and the US Environmental Protection Agency under STAR Agreement RD-833749. It has not been formally reviewed by the EPA. The views expressed in this document are solely those of the authors and the EPA does not endorse any products or commerical services mentioned in this publication.

References

Aiken, A. C., DeCarlo, P. F., and Jimenez, J. L.: Elemental analysis of organic species with electron ionization high-resolution mass spectrometry, Anal. Chem., 79, 8350–8358, 2007.

9476
Aiken, A. C., Decarlo, P. F., Kroll, J. H., Worsnop, D. R., Huffman, J. A., Docherty, K. S., Ulbrich, I. M., Mohr, C., Kimmel, J. R., Sueper, D., Sun, Y., Zhang, Q., Trimborn, A., Northway, M., Ziemann, P. J., Canagaratna, M. R., Onasch, T. B., Alfarra, M. R., Prevot, A. S. H., Dommen, J., Duplissy, J., Metzger, A., Baltensperger, U., and Jimenez, J. L.: O/C and OM/OC ratios of primary, secondary, and ambient organic aerosols with high-resolution time-of-flight aerosol mass spectrometry, Environ. Sci. Technol., 42, 4478–4485, 2008. 9476
Bahreini, R., Keywood, M. D., Ng, N. L., Varutbangkul, V., Gao, S., Flagan, R. C., Seinfeld, J. H., Worsnop, D. R., and Jimenez, J. L.: Measurements of secondary organic aerosol from oxidation of cycloalkenes, terpenes, and m-xylene using an aerodyne aerosol mass spectrometer, Environ. Sci. Technol., 39, 5674–5688, 2005. 9460
Bilde, M. and Pandis, S. N.: Evaporation rates and vapor pressures of individual aerosol species formed in the atmospheric oxidation of alpha- and beta-pinene, Environ. Sci. Technol., 35, 3344–3349, 2001. 9463
Canagaratna, M. R., Jayne, J. T., Jimenez, J. L., Allan, J. D., Alfarra, M. R., Zhang, Q., Onasch, T. B., Drewnick, F., Coe, H., Middlebrook, A., Delia, A., Williams, L. R., Trimborn, A. M., Northway, M. J., DeCarlo, P. F., Kolb, C. E., Davidovits, P., and Worsnop, D. R.: Chemical and microphysical characterization of ambient aerosols with the aerodyne aerosol mass spectrometer, Mass. Spec. Rev., 26, 185–222, 2007. 9476
Chan, A. W. H., Kroll, J. H., Ng, N. L., and Seinfeld, J. H.: Kinetic modeling of secondary organic aerosol formation: effects of particle- and gas-phase reactions of semivolatile products, Atmos. Chem. Phys., 7, 4135–4147, 2007, http://www.atmos-chem-phys.net/7/4135/2007/. 9473
Chen, J. J. and Griffin, R. J.: Modeling secondary organic aerosol formation from oxidation of alpha-pinene, beta-pinene, and d-limonene, Atmos. Environ., 39, 7731–7744, 2005. 9465
Claeys, M., Iinuma, Y., Szmigielski, R., Surratt, J. D., Blockhuys, F., Van Alsenoy, C., Böge, O., Sierau, B., Gómez-González, Y., Vermeylen, R., Van der Veken, P., Shahgholi, M., Chan, A. W. H., Herrmann, H., Seinfeld, J. H., and Maenhaut, W.: Terpenylic acid and related compounds from the oxidation of α-pinene: Implications for new particle formation and growth above forests, submitted, 2009. 9467, 9481
Cocker, D. R., Flagan, R. C., and Seinfeld, J. H.: State-of-the-art chamber facility for studying atmospheric aerosol chemistry, Environ. Sci. Technol., 35, 2594–2601, 2001. 9475
DeCarlo, P. F., Kimmel, J. R., Trimborn, A., Northway, M. J., Jayne, J. T., Aiken, A. C., Go-

nin, M., Fuhrer, K., Horvath, T., Docherty, K. S., Worsnop, D. R., and Jimenez, J. L.: Field-deployable, high-resolution, time-of-flight aerosol mass spectrometer, Anal. Chem., 78, 8281–8289, 2006. 9476

Docherty, K. S., Wu, W., Lim, Y. B., and Ziemann, P. J.: Contributions of organic peroxides to secondary aerosol formed from reactions of monoterpenes with O_3, Environ. Sci. Technol., 39, 4049–4059, 2005. 9463, 9467, 9468

Donahue, N. M., Robinson, A. L., Stanier, C. O., and Pandis, S. N.: Coupled partitioning, dilution, and chemical aging of semivolatile organics, Environ. Sci. Technol., 40, 2635–2643, 2006. 9462

Dzepina, K., Volkamer, R. M., Madronich, S., Tulet, P., Ulbrich, I. M., Zhang, Q., Cappa, C. D., Ziemann, P. J., and Jimenez, J. L.: Evaluation of new secondary organic aerosol models for a case study in Mexico City, Atmos. Chem. Phys. Discuss., 9, 4417–4488, 2009, http://www.atmos-chem-phys-discuss.net/9/4417/2009/. 9471

Gao, S., Keywood, M., Ng, N. L., Surratt, J., Varutbangkul, V., Bahreini, R., Flagan, R. C., and Seinfeld, J. H.: Low-molecular-weight and oligomeric components in secondary organic aerosol from the ozonolysis of cycloalkenes and alpha-pinene, J. Phys. Chem. A., 108, 10147–10164, 2004. 9466

Hallquist, M., Wenger, J. C., Baltensperger, U., Rudich, Y., Simpson, D., Claeys, M., Dommen, J., Donahue, N. M., George, C., Goldstein, A. H., Hamilton, J. F., Herrmann, H., Hoffmann, T., Iinuma, Y., Jang, M., Jenkin, M., Jimenez, J. L., Kiendler-Scharr, A., Maenhaut, W., McFiggans, G., Mentel, Th. F., Monod, A., Prvt, A. S. H., Seinfeld, J. H., Surratt, J. D., Szmigielski, R., and Wildt, J.: The formation, properties and impact of secondary organic aerosol: current and emerging issues, Atmos. Chem. Phys. Discuss., 9, 3555–3762, 2009, http://www.atmos-chem-phys-discuss.net/9/3555/2009/. 9472

Iinuma, Y., Boge, O., Gnauk, T., and Herrmann, H.: Aerosol-chamber study of the alpha-pinene/O-3 reaction: influence of particle acidity on aerosol yields and products, Atmos. Environ., 38, 761–773, 2004. 9466

Jenkin, M. E.: Modelling the formation and composition of secondary organic aerosol from α- and β-pinene ozonolysis using MCM v3, Atmos. Chem. Phys., 4, 1741–1757, 2004, http://www.atmos-chem-phys.net/4/1741/2004/. 9463, 9465

Keywood, M. D., Varutbangkul, V., Bahreini, R., Flagan, R. C., and Seinfeld, J. H.: Secondary organic aerosol formation from the ozonolysis of cycloalkenes and related compounds, Environ. Sci. Technol., 38, 4157–4164, 2004. 9475

Kroll, J. H. and Seinfeld, J. H.: Representation of secondary organic aerosol laboratory chamber data for the interpretation of mechanisms of particle growth, Environ. Sci. Technol., 39, 4159–4165, 2005. 9466, 9472

Kroll, J. H. and Seinfeld, J. H.: Chemistry of secondary organic aerosol: Formation and evolution of low-volatility organics in the atmosphere, Atmos. Environ., 42, 3593–3624, 2008. 9472

Müller, L., Reinnig, M. C., Warnke, J., and Hoffmann, T.: Unambiguous identification of esters as oligomers in secondary organic aerosol formed from cyclohexene and cyclohexene/α-pinene ozonolysis, Atmos. Chem. Phys., 8, 1423–1433, 2008, http://www.atmos-chem-phys.net/8/1423/2008/. 9466, 9470

Ng, N. L., Kroll, J. H., Keywood, M. D., Bahreini, R., Varutbangkul, V., Flagan, R. C., Seinfeld, J. H., Lee, A., and Goldstein, A. H.: Contribution of first- versus second-generation products to secondary organic aerosols formed in the oxidation of biogenic hydrocarbons, Environ. Sci. Technol., 40, 2283–2297, 2006. 9464, 9465, 9471, 9482, 9483

Odum, J. R., Hoffmann, T., Bowman, F., Collins, D., Flagan, R. C., and Seinfeld, J. H.: Gas/particle partitioning and secondary organic aerosol yields, Environ. Sci. Technol., 30, 2580–2585, 1996. 9458, 9459

Pankow, J. F.: An absorption-model of gas-particle partitioning of organic-compounds in the atmosphere, Atmos. Environ., 28, 185–188, 1994a. 9458, 9473

Pankow, J. F.: An absorption-model of the gas aerosol partitioning involved in the formation of secondary organic aerosol, Atmos. Environ., 28, 189–193, 1994b. 9458, 9473

Pankow, J. F. and Asher, W. E.: SIMPOL.1: a simple group contribution method for predicting vapor pressures and enthalpies of vaporization of multifunctional organic compounds, Atmos. Chem. Phys., 8, 2773–2796, 2008, http://www.atmos-chem-phys.net/8/2773/2008/. 9463, 9466, 9481

Pankow, J. F. and Chang, E. I.: Variation in the sensitivity of predicted levels of atmospheric organic particulate matter (OPM), Environ. Sci. Technol., 42, 7321–7329, 2008. 9474

Pankow, J. F., Seinfeld, J. H., Asher, W. E., and Erdakos, G. B.: Modeling the formation of secondary organic aerosol. 1. Application of theoretical principles to measurements obtained in the alpha-pinene/, beta- pinene/, sabinene/, Delta(3)-carene/, and cyclohexene/ozone systems, Environ. Sci. Technol., 35, 1164–1172, 2001. 9461, 9462

Pathak, R. K., Stanier, C. O., Donahue, N. M., and Pandis, S. N.: Ozonolysis of alpha-pinene at atmospherically relevant concentrations: Temperature dependence of aerosol mass fractions

(yields), J. Geophys. Res.-Atmos., 112, D03201, doi:10.1029/2006JD007436, 2007. 9464, 9465, 9466, 9482, 9483

Presto, A. A. and Donahue, N. M.: Investigation of alpha-pinene plus ozone secondary organic aerosol formation at low total aerosol mass, Environ. Sci. Technol., 40, 3536–3543, 2006. 9464

Seinfeld, J. H., Erdakos, G. B., Asher, W. E., and Pankow, J. F.: Modeling the formation of secondary organic aerosol (SOA). 2. The predicted effects of relative humidity on aerosol formation in the alpha-pinene-, beta-pinene-, sabinene-, Delta(3)-Carene-, and cyclohexene-ozone systems, Environ. Sci. Technol., 35, 1806–1817, 2001. 9461

Shilling, J. E., Chen, Q., King, S. M., Rosenoern, T., Kroll, J. H., Worsnop, D. R., McKinney, K. A., and Martin, S. T.: Particle mass yield in secondary organic aerosol formed by the dark ozonolysis of alpha-pinene, Atmos. Chem. Phys., 8, 2073–2088, 2008, http://www.atmos-chem-phys.net/8/2073/2008/. 9460, 9464, 9465, 9470, 9482, 9483, 9486

Shilling, J. E., Chen, Q., King, S. M., Rosenoern, T., Kroll, J. H., Worsnop, D. R., DeCarlo, P. F., Aiken, A. C., Sueper, D., Jimenez, J. L., and Martin, S. T.: Loading-dependent elemental composition of α-pinene SOA particles, Atmos. Chem. Phys., 9, 771–782, 2009, http://www.atmos-chem-phys.net/9/771/2009/. 9465, 9468, 9469, 9470, 9471, 9487

Stanier, C. O., Donahue, N., and Pandis, S. N.: Parameterization of secondary organic aerosol mass fractions from smog chamber data, Atmos. Environ., 42, 2276–2299, 2008. 9461, 9462

Yu, J. Z., Cocker, D. R., Griffin, R. J., Flagan, R. C., and Seinfeld, J. H.: Gas-phase ozone oxidation of monoterpenes: Gaseous and particulate products, J. Atmos. Chem., 34, 207–258, 1999. 9463, 9467, 9468, 9484, 9485

Table 1. Major products chosen to represent the ozonolysis of α-pinene under dry, dark, and low-NO_x conditions in the presence of dry ammonium sulfate particles.

				Product-Specific Model				Volatility Basis Set		
				(K_p × 1 case)		(K_p × 100 case)				
Product	**Chemical structure**	**O/C**	**H/C**	**K_p[a] (c^*)**	**α**	**K_p (c^*)**	**α**	**K_p (c^*)**	**α**	**α from Product-Specific Model (K_p × 100 case)**
Pinic acid $C_9H_{14}O_4$ (MW: 186)		0.444	1.556	0.2822 (3.544)	0.2308	28.22 (0.0354)	0.0563	100 (0.01)	0.0707	0.0563 (Pinic acid: c^* = 0.0354)
Terpenylic acid [b] $C_8H_{12}O_4$ (MW: 172)		0.5	1.5	0.0332 (30.12)	0.0172	3.32 (0.3012)	0.0132	10 (0.1)	0.0110	0.0131 (Terpenylic acid: c^* = 0.3012)
Hydroperoxide $C_{10}H_{16}O_4$ (MW: 200)		0.4	1.6	0.0029 (344.8)	0.0181	0.29 (3.448)	0.0173	1 (1)	0.0120	0.0172 (Hydroperoxide: c^* = 3.448)
Pinonic acid $C_{10}H_{16}O_3$ (MW: 184)		0.3	1.6	0.0018 (555.6)	0.6883	0.18 (5.556)	0.1573	0.1 (10)	0.1603	0.1573 (Pinonic acid: c^* = 5.556)
								0.01 (100)	0.0210	-
Pinonaldehyde $C_{10}H_{16}O_2$ (MW: 168)		0.2	1.6	1.145×10^{-5} (87334)	1	1.145×10^{-3} (873.34)	0.9380	0.001 (1000)	0.9554	0.9380 (Pinonaldehyde: c^* = 873.34)

[a] Vapor pressure is determined at 293 K using a model developed by Pankow and Asher (2008). K_p is determined at 293 K with the assumption of activity coefficient of the products equal to one and the molecular weight of product i, is used as mean molecular weight in organic absorbing phase, as a first approximation.

[b] (Claeys et al., 2009)

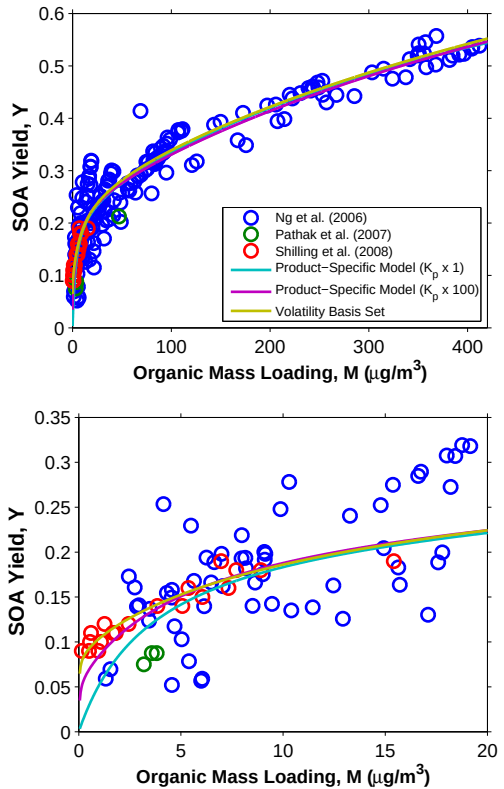

Fig. 1. SOA yield from ozonolysis of α-pinene at different organic mass loading, M. Data represent experiments conducted under dry, dark, and low-NO_x conditions in the presence of dry ammonium sulfate particles (Ng et al., 2006; Pathak et al., 2007; Shilling et al., 2008). Top panel: organic mass loading: 0–411 μg m^{-3}; Bottom panel: organic mass loading: 0–20 μg m^{-3}. SOA yield data are adjusted to 293 K, using a temperature correction factor. Lines show the model fit with the parameters given in Table 1.

ACPD
9, 9457–9489, 2009

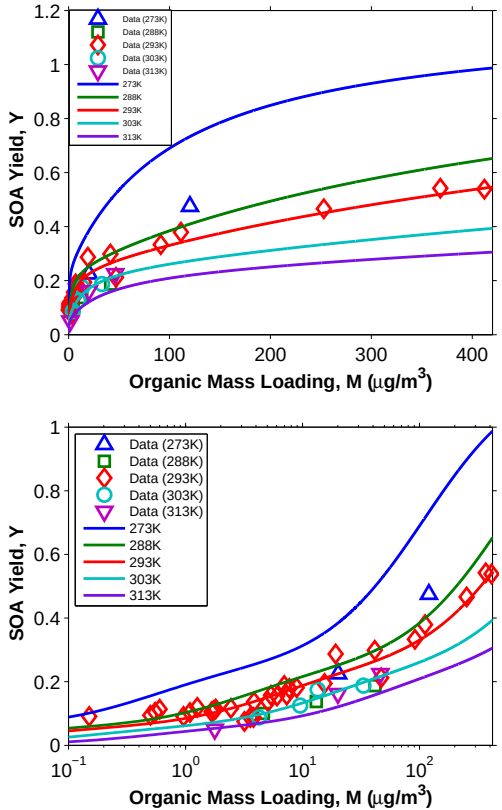

Fig. 2. Temperature dependence of SOA yield of ozonolysis of α-pinene obtained from experiments conducted under dry, dark, and low-NO_x conditions in the presence of dry ammonium sulftae particles. Data (293 K) are the final SOA yields from Ng et al. (2006), Pathak et al. (2007) and Shilling et al. (2008). Data from Shilling et al. (2008) have been adjusted to 293 K. Data at other temperatures are obtained from Pathak et al. (2007). The lines show the model fit at different temperatures for the $K_p \times 100$ case.

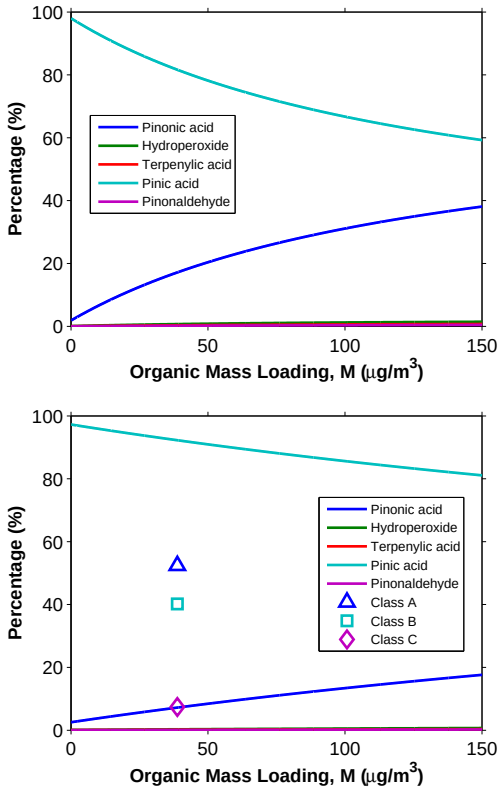

Fig. 3. Relative contributions of the modeled products to the SOA yield at different organic mass loadings for $K_p \times 1$ case at different temperatures. Top panel: 293 K; Bottom panel: 306 K; Class A refers to the sum of the percentages of pinonic acid, norpinonic acid and isomers, and hydroxy pinonaldehyde (Yu et al., 1999); Class B refers to the sum of the percetages of pinic acid, norpinic acid, and hydroxy pinonic acid (Yu et al., 1999); Class C refers to the sum of the percentages of pinonaldehyde and norpinonaldehyde (Yu et al., 1999).

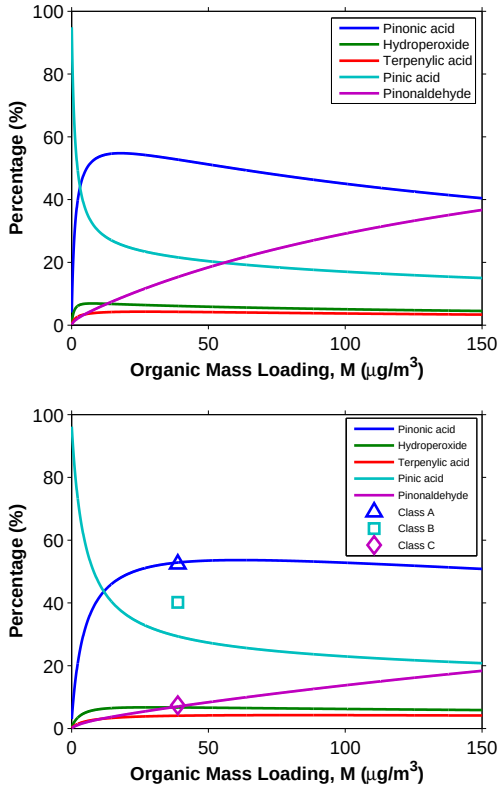

Fig. 4. Relative contributions of the modeled products to the SOA yield at different organic mass loadings for $K_p \times 100$ case at different temperatures. Top panel: 293 K; Bottom panel: 306 K; Class A refers to the sum of the percentages of pinonic acid, norpinonic acid and isomers, and hydroxy pinonaldehyde (Yu et al., 1999); Class B refers to the sum of the percetages of pinic acid, norpinic acid, and hydroxy pinonic acid (Yu et al., 1999); Class C refers to the sum of the percentages of pinonaldehyde and norpinonaldehyde (Yu et al., 1999).

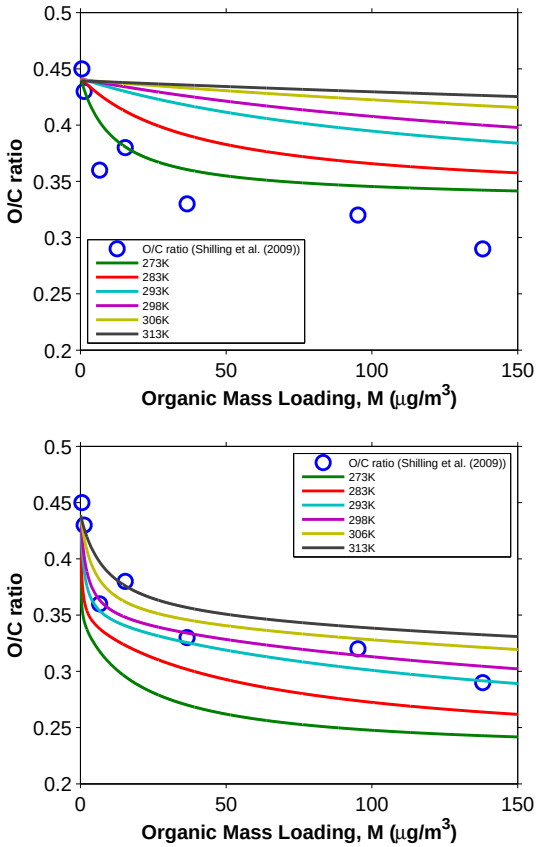

Fig. 5. O/C ratio of SOA formed from the ozonolysis of α-pinene under dry, dark, and low-NO_x conditions in the presence of dry ammonium sulfate particles as a function of organic mass laoding, M, at different temperatures. Top panel: $K_p \times 1$ case; Bottom panel: $K_p \times 100$ case; Blue open circles represent measured O/C ratios reported by Shilling et al. (2008) at 298 K.

ACPD
9, 9457–9489, 2009

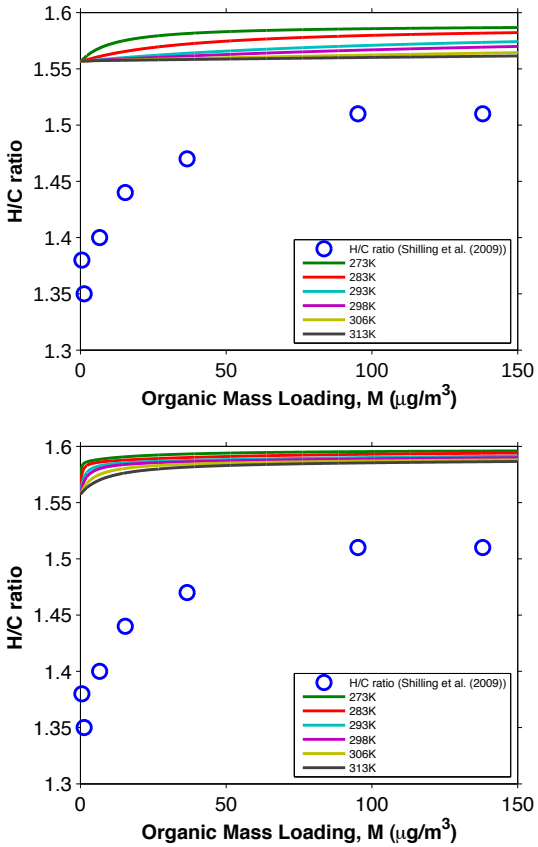

Fig. 6. H/C ratio of SOA formed from the ozonolysis of α-pinene under dry, dark, and low-NO_x conditions in the presence of dry ammonium sulfate particles as a function of organic mass loading, M, at different temperatures. Top panel: $K_p \times 1$ case; Bottom panel: $K_p \times 100$ case; Blue open circles represent measured H/C ratios reported by Shilling et al. (2009) at 298 K.

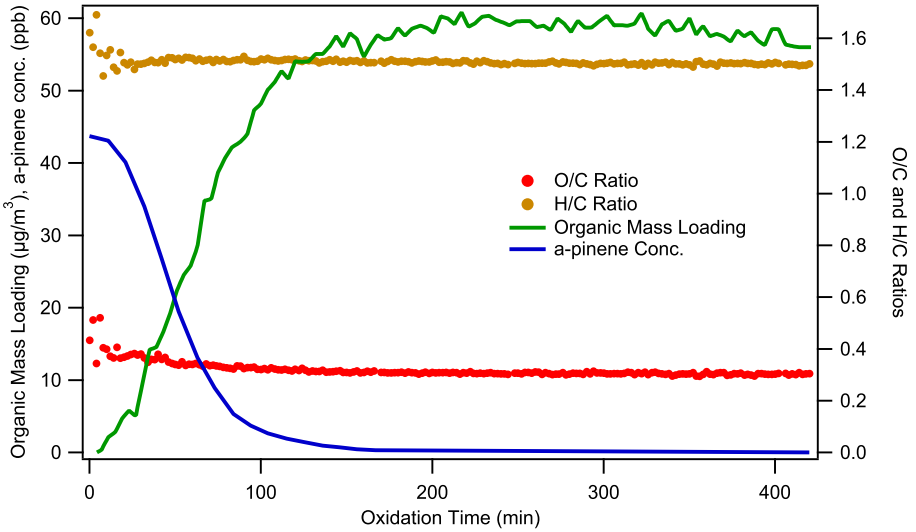

Fig. 7. Time evolution of α-pinene concentration, organic mass loading, and O/C and H/C ratios during ozonolysis of α-pinene under dry, dark, and low-NO_x conditions in the presence of dry ammonium sulfate particles. Experiment conducted in the Caltech laboratory chamber. Conditions given in Appendix B.

ACPD
9, 9457–9489, 2009

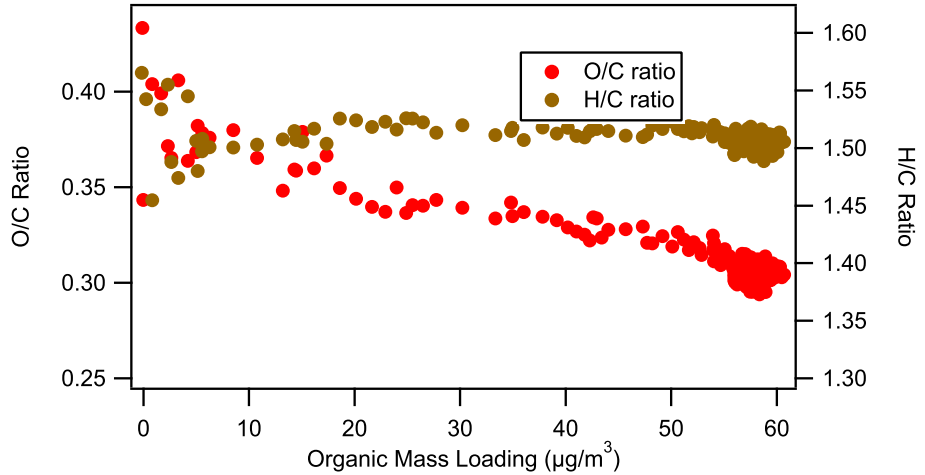

Fig. 8. O/C and H/C ratios of SOA formed from the ozonolysis of α-pinene under dry, dark, and low-NO_x conditions in the presence of dry ammonium sulfate particles as function of organic mass loading, M. Experiment conducted in the Caltech laboratory chamber. Conditions given in Appendix B.

ACPD
9, 9457–9489, 2009